Ultrafast Excited-State Dynamics of $Re(CO)_3Cl(dcbpy)$ in Solution and on Nanocrystalline TiO_2 and ZrO_2 Thin Films

Yongqiang Wang, John B. Asbury, and Tianquan Lian*

Department of Chemistry, Emory University, Atlanta, Georgia 30322

Received: October 13, 1999; In Final Form: January 25, 2000

Femtosecond infrared spectroscopy was used to study the excited-state dynamics of $Re(CO)_3Cl(dcbpy)$ in DMF solution and on the surface of ZrO_2 and TiO_2 nanocrystalline thin films. For $Re(CO)_3Cl(dcbpy)$ in DMF solution, we observed a long-lived ^{3}MLCT state with a lifetime of >1 ns. The frequencies for the CO stretching bands were blue-shifted compared to those in the ground state, consistent with the metal-to-ligand charge-transfer nature of the excited state. Rapid spectral evolution of the excited-state CO stretching bands was observed within the first 12 ps. For $Re(CO)_3Cl(dcbpy)$ on ZrO_2 thin films, a similar ^{3}MLCT state was observed. However, the spectral blue shift was much less pronounced and occurred on a faster time scale. We suggest that vibrational relaxation is the primary contribution to the spectral evolution of $Re(CO)_3Cl(dcbpy)$ on the ZrO_2 film, whereas both vibrational relaxation and solvation of the MLCT state contribute to the spectral evolution in DMF solution. The excited-state decay rate of $Re(CO)_3Cl(dcbpy)$ on ZrO_2 films was faster than the rate in DMF and increased with higher excitation power. The faster excited-state decay is attributed to the occurrence of an excited-state quenching process between neighboring excited molecules on the film. For $Re(CO)_3Cl(dcbpy)$-sensitized TiO_2 thin films, broad mid-IR absorption of injected electrons was observed. The rise time of the electron absorption signal in TiO_2 was found to be less than 100 fs. In addition, the adsorbate CO stretching bands were also observed. We discuss the detailed information about the electron-injection process that can be obtained from the adsorbate vibrational spectra.

1. Introduction

Interfacial electron transfer (ET) between semiconductor nanoparticles and molecular adsorbates has been a subject of intense research interest in recent years.[1−4] This fundamental process is directly related to the application of semiconductor nanomaterials to photography,[5] solar energy conversion,[6] and photocatalysis.[7] Since the report by Graetzel's group that solar cells based on nanocrystalline TiO_2 thin films sensitized by $Ru(dcbpy)_2(NCS)_2$ (dcbpy = 4,4′-dicarboxy-2,2′-bipyridine) (referred to as RuN3) can achieve a solar-to-electric power conversion efficiency of about 10%,[8,9] the electron-injection and recombination properties of Ru-dye-sensitized semiconductor nanoparticles have been studied by many groups.[10−26] Many recent studies of RuN3 and related dyes on the TiO_2 surface have reported ultrafast electron injection from the excited state of the dye to TiO_2 on the 100-fs or faster time scale.[11−15,17,27,28] Back ET from TiO_2 to RuN3 was determined to be in the millisecond to microsecond time scale.[17,29] The fast electron injection and slow back-ET time ensure a large incident-photon-to-current conversion efficiency.

The detailed mechanism of the fast electron-injection process is still unclear. The reported ultrafast electron injection from RuN3 to TiO_2 occurs on a time scale that is the same as or faster than that of vibrational and electronic relaxation in the excited state. Whether electron injection occurs from a vibrationally hot state has not been unambiguously determined, although the <100-fs injection time is very suggestive of that possibility. Our recent study of a series of Ru dyes, $Ru(dcbpy)_2X_2$ where X = NCS, CN, Cl, or dcbpy,[30] found that the apparent electron-injection rates in this series of dyes were similar, but that the electron-injection quantum yields were different. These sensitizers, which share common carboxylic acid groups anchoring them to the nanoparticle surface, should exhibit very similar electronic coupling to TiO_2. The main differences among these dyes are the relative redox potentials of their excited states. This result may suggest that there is a competition between the electron-injection and vibrational- or electronic-relaxation pathways and that the branching ratio between them may determine the overall injection quantum yield. To gain a more detailed understanding of the ultrafast electron-injection step, we need to directly assess both the electron-injection and the excited-state-relaxation pathways.

Transient mid-IR spectroscopy has been used to study electron transfer in sensitized nanoparticles.[10−13,31−33] We recently demonstrated that this technique can simultaneously probe both the injected electrons in TiO_2 and the vibrational spectra of the adsorbate.[32] Injected electrons in TiO_2 nanoparticles were shown to have a very broad absorption in the $4-6\ \mu$m region.[10−13,31−33] We have also observed a similar broad mid-IR absorption of electrons in other semiconductor nanoparticles, such as ZnO[33] and CdS. Although the full spectrum and exact origin of the transitions of the broad electron absorption have not been fully examined in nanoparticles, they are well understood in bulk[34,35] and quantum-well[36] semiconductor materials. This absorption consists of free carrier absorption,[37] which is often broad and which increases with wavelength, intraband transitions[37] between different valleys (or subbands) within the conduction band, and absorptions of trap states. Because the IR absorption of electrons is direct evidence for the arrival of electrons inside semiconductor nanoparticles, it provides an unambiguous spectroscopic

* To whom correspondence should be addressed. E-mail: tlian@emory.edu.

10.1021/jp9936648 CCC: $19.00
Published on Web 03/22/2000

probe for the study of interfacial electron transfer between a semiconductor and its adsorbates.

We and other groups have recently studied electron-transfer dynamics in RuN3 and related dye-sensitized TiO_2 thin films using femtosecond mid-IR spectroscopy.[11−13] We directly determined the electron-injection time by monitoring the broad mid-IR absorption of injected electrons in TiO_2. However, the IR absorption cross section of electrons is much larger than that of the adsorbate vibrational bands. As a result, we were not able to simultaneously obtain the transient IR spectrum of the SCN stretching mode. In an effort to obtain more insight into the electron-injection process, an alternative sensitizer with strong adsorbate vibrational bands but similar structure is needed. $Re(CO)_3Cl(dcbpy)$ (dcbpy = 4,4′-dicarboxy-2,2′-bipyridine) (referred to as ReCO from this point on) appears to be a good candidate. In a manner similar to that in RuN3-sensitized TiO_2,[12] the optical absorption in the Re complex is dominated by a Re-to-dcbpy metal-to-ligand charge-transfer (MLCT) band. In the MLCT state, electron injection to TiO_2 may occur through the π^* orbital of the dcbpy ligand. In this system, there are three strong CO stretching bands that can be used as a probe of the adsorbate dynamics. In this paper, we will report our recent transient IR study of $Re(CO)_3Cl(dcbpy)$ in solution and on the surface of ZrO_2 and TiO_2 nanocrystalline thin films.

2. Experimental Section

Femtosecond IR Spectrometer. The femtosecond IR spectrometer used in these experiments is based on an amplified femtosecond Ti:sapphire laser system from Clark-MXR (1-kHz repetition rate at 800 nm, 100-fs pulse width, 900 μJ/pulse). Nonlinear frequency-mixing techniques are used to generate mid-infrared probe pulses and UV pump pulses, the details of which have been described elsewhere.[32] Briefly, the 800-nm output is split into two beams at 500 and 400 μJ/pulse. The 500-μJ/pulse beam is used to pump an optical parametric amplifier to generate two near-infrared pulses at about 1.5 and 1.9 μm. These two pulses are then mixed in a $AgGaS_2$ crystal to generate mid-infrared light at about a 5-μm wavelength. The mid-infrared probe pulse has a bandwidth greater than 200 cm^{-1} and is dispersed into an imaging spectrograph, where it is imaged onto an infrared HgCdTe(MCT) array detector and digitized by a scheme described below. The other, 400-μJ/pulse fundamental beam is attenuated with a variable neutral density filter and frequency doubled in a BBO crystal to make 400-nm pulses.

In all of the experiments presented here, a moving solution or film sample was pumped at 5 μJ of 400-nm light, unless otherwise noted, and the subsequent absorbance change was measured in the 1820−2200 cm^{-1} region. The diameters of the pump and probe beams were 400 and 300 μm, respectively. The instrument response function, that is, the cross correlation of the pump and probe pulses, was measured in a thin silicon wafer, in which 400-nm excitation led to the instantaneous generation of free carriers that absorbed strongly in the mid-infrared region. The typical instrument response was well represented by a Gaussian function with a full width at half-maximum (fwhm) of less than 200 fs.

Infrared MCT Array Detector. The infrared MCT array detector used to detect the dispersed mid-infrared probe was obtained from EG&G Optoelectronics. The array consists of 32 0.5-mm-wide by 1-mm-tall HgCdTe elements arrayed horizontally with 25-μm spacing between each element. The detector output was amplified by a matching 32-channel amplifier, also obtained from EG&G Optoelectronics. The 32 amplifier output channels were captured by four 8-channel simultaneous sample-and-hold devices (Keithley model SSH8-FG) that were synchronized by and linked to an analog-to-digital converter card (Keithley model DAS 1801HC). The simultaneous sample-and-hold devices acquired all 32 amplifier output channels within a 2-ns window. A personal computer (Dell, 400-MHz Pentium II Processor) was used to collect and process the output from the analog-to-digital converter for every laser shot at a 1-kHz repetition rate. Differential absorbance measurements were calculated with adjacent pulses by blocking every other pump pulse with a synchronized optical chopper. Each element of the array averaged a 5-cm^{-1} slice of the infrared spectrum, so that the total spectral region covered by the array was about 160 cm^{-1}.

Sample Preparations. The TiO_2 nanoparticle thin films were prepared by a method similar to that used by Zaban and coworkers.[21] Briefly, the TiO_2 nanoparticle colloid was prepared by the controlled hydrolysis of titanium(IV) isopropoxide in a mixture of glacial acetic acid and water at 0 °C. The resulting solution was heated to 80 °C for 8 h and then autoclaved at 230 °C for 12 h. The resulting colloid was concentrated to 150 g/L, spread onto polished sapphire windows, and baked at 400 °C for 36 min. The ZrO_2 nanocrystalline thin films were prepared by a previously described method,[8] using ZrO_2 nanoparticles obtained from Degussa Corporation.

The synthesis of the complex $Re(CO)_3Cl(dcbpy)$ (dcbpy = 4,4′-dicarboxy-2,2′-bipyridine) will be described in detail elsewhere.[38] The solution sample in dimethylformamide (DMF) was prepared by dissolving ReCO to a concentration of 1.8 mM. The solution was stable for several days in the dark. The solution sample cell had a path length of 250 μm. The ZrO_2 and TiO_2 film samples were prepared by soaking the films in a solution of 1.8 mM ReCO in DMF for 10 h. The thin-film and solution samples were scanned rapidly during measurements to prevent any long-term photoproduct buildup.

3. Results

ReCO in DMF. The transient absorption spectra of ReCO in DMF solution are shown in panels a and b of Figure 1. Figure 1a shows the transient spectra at 1.5, 12, 96, and 831 ps after 400-nm excitation. The three bleach peaks at 1899, 1914, and 2019 cm^{-1} correspond to the three CO stretching bands in the static FTIR spectrum of ReCO in DMF, shown as the thin dotted line in Figure 1a. The excited-state absorption peaks fully develop at 1959, 1998, and 2073 cm^{-1} after 12 ps. Before this time, rapid spectral evolution occurs. Figure 1b shows transient absorption spectra of ReCO in DMF at 1, 2, 4, 7, and 12 ps. The bleach features have been cropped in this figure to highlight the spectral evolution of the excited-state CO absorption bands. The spectral evolution can most clearly be seen around the CO stretching band at 2073 cm^{-1}.

Panels a and b of Figure 2 show the transient bleach-recovery and absorption-decay kinetics of the ground-state bleach at 1899 cm^{-1} and the excited-state absorption at 2073 cm^{-1}, respectively. The traces have been normalized to unit signal magnitude. The ground-state bleach recovery at 1899 cm^{-1}, shown in Figure 2a, was fit to a single-exponential recovery having a lifetime of approximately 2 ns. The lifetime could not be determined accurately because of the limited delay time (<1 ns). The excited-state absorption decay at 2073 cm^{-1}, shown in Figure 2b, was also fit to a single-exponential decay having a lifetime of about 10 ns. The formation kinetics of the absorption band at 2073 cm^{-1} are shown as open circles in Figure 4. It is well fit by an exponential rise function with a 4-ps time constant, shown by the solid line in Figure 4.

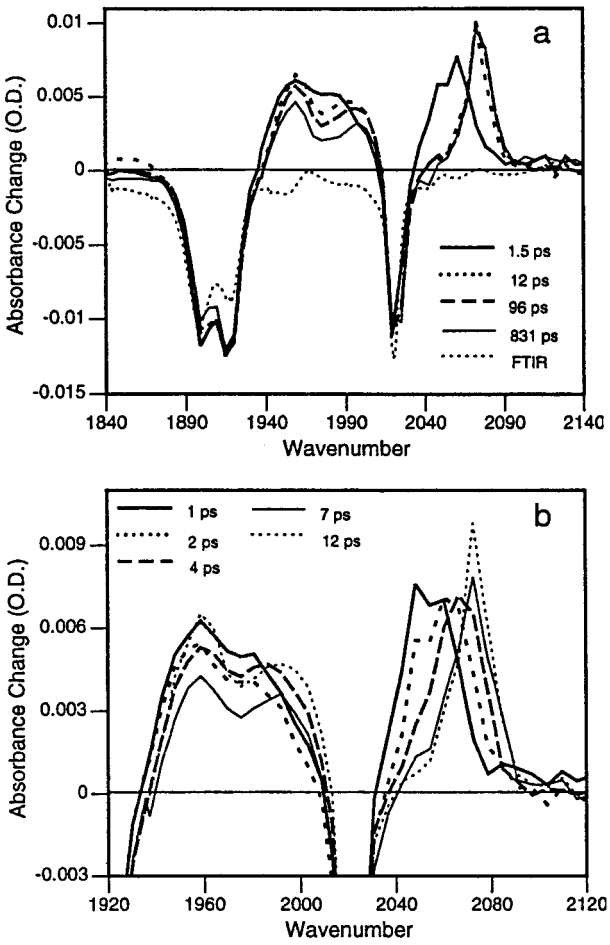

Figure 1. (a) Transient IR difference spectra of ReCO in DMF at 1.5 (thick solid line), 12 (thick dotted line), 96 (thick dashed line), and 831 ps (thin solid line) after 400-nm excitation. The FTIR spectrum of ReCO in DMF is shown as the thin dotted line. (b) Transient IR difference spectra of ReCO in DMF at 1 (thick solid line), 2 (thick dotted line), 4 (thick dashed line), 7 (thin solid line), and 12 ps (thin dotted line) after 400-nm excitation.

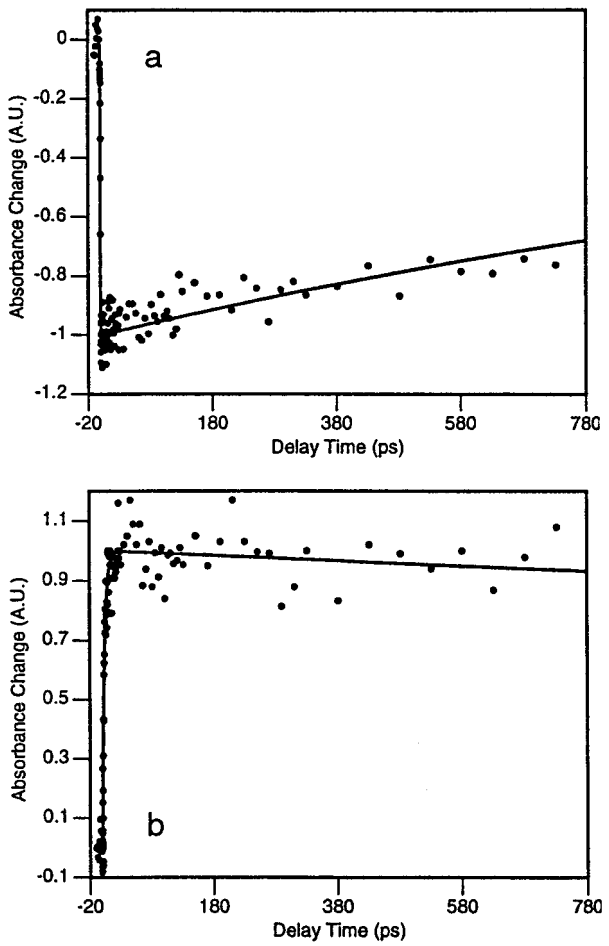

Figure 2. Normalized kinetics traces of ReCO in DMF measured at the peaks of the low-frequency bleach and high-frequency absorption (a) at 1899 cm^{-1} fit with a ~2-ns single-exponential recovery and (b) at 2073 cm^{-1} fit with a ~10-ns single-exponential decay.

ReCO on a ZrO_2 Film. The ReCO complex was adsorbed onto the surface of a ZrO_2 nanocrystalline thin film to investigate its photophysics on a dry, noninjecting substrate surface. The transient absorption spectra collected 1.5, 12, 96, and 831 ps after 400 nm excitation are shown in Figure 3a. Shown in Figure 3b is the early-time spectral evolution. In this figure, the ground-state bleach peaks have been cropped to focus on the excited-state absorption dynamics. As shown in Figure 3a, the three bleach peaks at 1917, 1944, and 2044 cm^{-1} correspond to the ground-state CO stretching bands of ReCO on ZrO_2 thin films, which are indicated in the static FTIR spectrum. Like ReCO in DMF, the excited-state CO stretching frequencies of ReCO on the ZrO_2 film, centered at ~1990 and 2069 cm^{-1}, are blue-shifted relative to the ground-state peaks. The two low-frequency excited-state CO absorption peaks are not well separated in the transient spectra. Instead, there appears only a single broad peak centered at 1990 cm^{-1}, which probably consists of the two overlapping CO stretching bands of the excited state. The high-frequency CO stretching band at 2069 cm^{-1} is clearly resolved in Figure 3a. As shown in Figure 3b, there appears to be much less of a spectral shift in the CO stretching frequency at early times compared to that of the complex in DMF. The formation time of the excited-state peak at 2069 cm^{-1}, which reflects the rate of the spectral shift, is shown by the solid circles in Figure 4. The rise time is roughly described by a single-exponential rise function with a 1.7-ps time constant.

To investigate the extent of excited-state quenching of the ReCO complex on the ZrO_2 nanocrystalline thin film, we measured the transient bleach-recovery and absorption-decay kinetics at three different pump energies, namely, 10, 5, and 2 μJ. The signal magnitudes scaled linearly with the pump energy, which is consistent with a single-photon process. Also, the bleach-recovery kinetics at all three bleach wavelengths for a given pump energy were the same within the limit of the noise. However, the bleach recovery was faster at the higher pump energy. The same was true for absorption-decay traces collected at around 1990 and 2069 cm^{-1}, the two excited-state absorption features. Panels a and b of Figure 5 shows the bleach-recovery kinetics at 2044 cm^{-1} and the absorption decay kinetics at 2069 cm^{-1} at the three pump energies. These frequencies were chosen because the signal-to-noise ratio of the kinetics was best. The bleach-recovery and absorption-decay kinetics were normalized to facilitate comparison and fit to single-exponential functions. As discussed later, the excited-state quenching process may be a bimolecular process, so the complete quenching kinetics cannot be well described by a single-exponential decay function. However, our data are limited to the <1-ns time range. In this limited time range and within the noise of the data, single-exponential fitting provides a convenient number for quantitatively comparing the quenching kinetics. The lifetimes of the single-exponential fits to the bleach-recovery kinetics shown

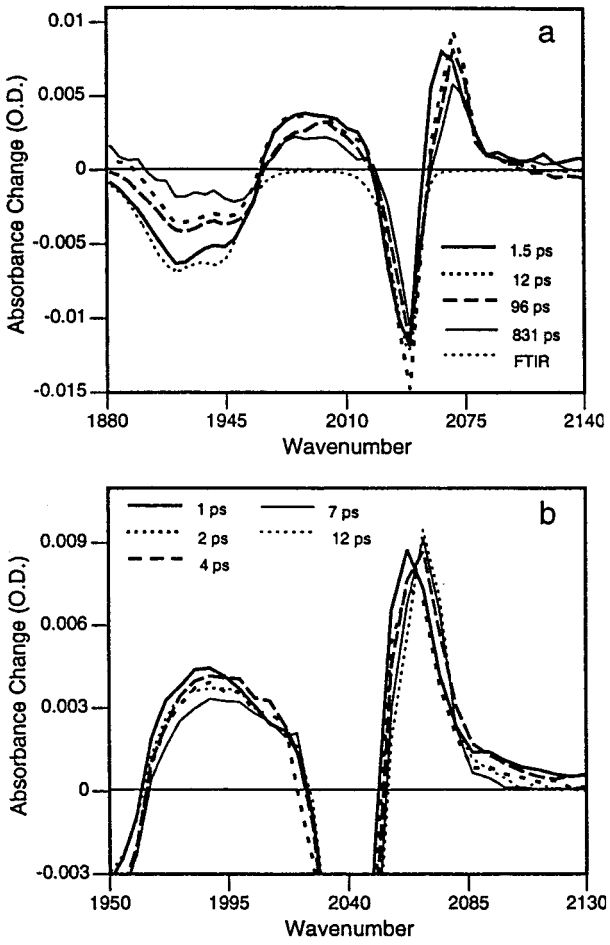

Figure 3. (a) Transient IR difference spectra of ReCO on a ZrO_2 nanocrystalline thin film at 1.5 (thick solid line), 12 (thick dotted line), 96 (thick dashed line), and 831 ps (thin solid line) after 400-nm excitation. The FTIR spectrum of ReCO on a ZrO_2 film is shown as the thin dotted line. (b) Transient IR difference spectra of ReCO on a ZrO_2 film at 1 (thick solid line), 2 (thick dotted line), 4 (thick dashed line), 7 (thin solid line), and 12 ps (thin dotted line) after 400-nm excitation.

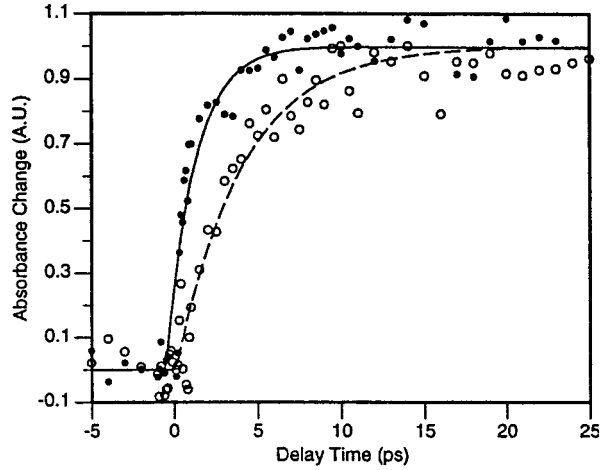

Figure 4. Comparison of the excited-state formation kinetics measured at 2069 cm^{-1} (solid circles) for ReCO on ZrO_2 and at 2073 cm^{-1} (open circles) for ReCO in DMF. Single-exponential fits (solid lines) of the data yield rise time constants of 1.7 ps on ZrO_2 and 4 ps in DMF solution.

in Figure 5a are 1.5, 4, and 7 ns for the 10-, 5-, and 2-μJ traces, respectively. The lifetimes of the single-exponential fits to the absorption-decay kinetics shown in Figure 5b are also 1.5, 4,

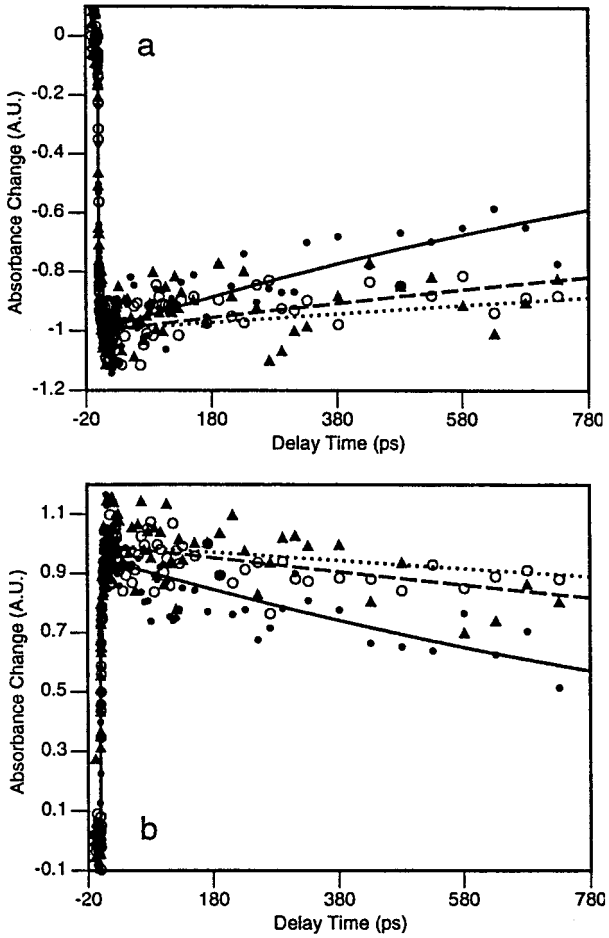

Figure 5. Comparison of the normalized kinetics traces of ReCO on a ZrO_2 nanocrystalline thin film measured at the high-frequency bleach and absorption peaks at 10- (solid circles), 5- (open circles), and 2-μJ (solid triangles) excitation energy. Panel (a) shows traces at 2044 cm^{-1} with single-exponential fits of the 10-, 5-, and 2-μJ traces having lifetimes of ~1.5 (solid line), ~4 (dashed line), and ~7 ns (dotted line), respectively. Panel (b) shows traces at 2069 cm^{-1} with single-exponential fits of the 10-, 5-, and 2-μJ traces having the same respective lifetimes.

and 7 ns for the 10-, 5-, and 2-μJ traces, respectively. Because of the long lifetime and small signal size, the exponential time constant for the data at the 2- and 5-μJ excitation powers is not accurately determined. Qualitatively, their lifetimes are longer than that at the 10-μJ excitation energy.

ReCO on a TiO_2 Film. Figure 6 shows the transient absorption spectra of the ReCO complex adsorbed onto the surface of a TiO_2 nanocrystalline thin film at 0.2−2 ps (solid line) and 500−1000 ps (dashed line) after 400-nm excitation. These spectra are focused on the region corresponding to the highest-frequency CO stretching mode. The spectra consist of a broad absorption that covers the entire spectral region interrogated by the probe, a pronounced bleach at 2040 cm^{-1} of the ground-state absorption of ReCO, and the corresponding excited-state absorption at 2070 cm^{-1}. The magnitude of the broad absorption is indicated by the flat thin dotted lines. In addition, there is also a small peak at around 2095 cm^{-1}. The static FTIR spectrum of ReCO on the nanocrystalline TiO_2 film is shown as the thin solid line in Figure 6. In addition, the transient absorption spectrum of ReCO on the ZrO_2 film at 831 ps has been included as the dotted line to facilitate assignment of the bands.

The rise time of the broad absorption was investigated at several wavelengths at higher frequency than the ground- and

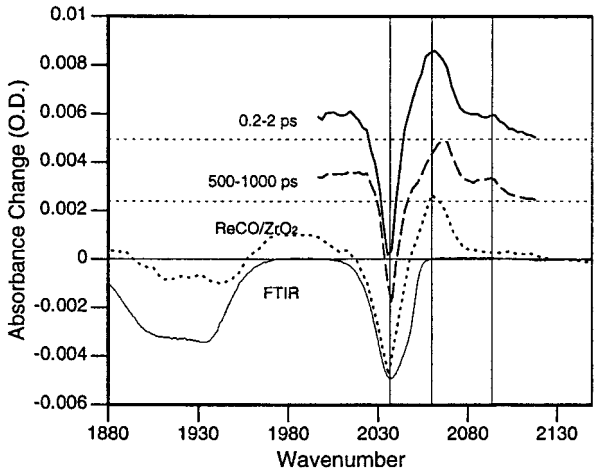

Figure 6. Transient IR difference spectra of ReCO on a TiO_2 nanocrystalline thin film at 0.2−2 ps (solid line) and 500−1000 ps (dashed line) after 400-nm excitation. The FTIR spectrum is shown as the thin solid line. The 831-ps difference spectrum of ReCO on a ZrO_2 nanocrystalline thin film is shown as the dotted dashed line.

excited-state absorptions. The dynamics of the broad absorption were the same within the limit of the noise across all probed frequencies on the blue side of the vibrational features of ReCO. Figure 7a shows a comparison of the transient signals at 2115 cm^{-1} from the TiO_2 film sensitized with ReCO (solid line) with the transient signals from the complex on a ZrO_2 film (dotted line) and from a naked TiO_2 film (dashed line) under the same excitation power. The rise time of the broad absorption at 2115 cm^{-1} is compared in Figure 7b with the instrument response function collected in a thin silicon wafer (dotted line), representing an instantaneous rise, and a 100-fs exponential rise convolved with the instrument response function (dashed line).

Figure 8a shows the decay of the broad absorption represented by the trace at 2115 cm^{-1} (solid triangles) compared with the traces at 2040 cm^{-1} (solid circles) and 2070 cm^{-1} (open circles), which correspond to the peaks of the ground- and excited-state absorptions, respectively, of the high-frequency CO stretching band. The decay traces were fit with two or three exponential components. The decay components for the three traces with relative amplitudes in parentheses are 10 ps (15%), 100 ps (35%), and ≫1 ns (50%) for the trace at 2115 cm^{-1}; 5 ps (27%), 100 ps (12%), and ≫1 ns (61%) for the trace at 2040 cm^{-1}; and 100 ps (29%) and >1 ns (71%) for the trace at 2070 cm^{-1}. The signal at 2040 cm^{-1} results from the superposition of the ground-state bleach on top of the broad absorption, and the signal at 2070 cm^{-1} results from the superposition of the excited-state absorption on top of the broad absorption. To separate the CO stretching signal from the broad absorption of electrons, we subtracted the trace at 2115 cm^{-1} (representing the broad absorption) from the trace at 2040 and 2070 cm^{-1}. The subtracted kinetics, shown in Figure 8b, represent the CO bleach-recovery dynamics at 2040 cm^{-1} (solid circles) and the excited-state decay dynamics at 2070 cm^{-1} (open circles) of the ReCO complex on the TiO_2 film. The trace has been fit to single- and biexponential functions having the following lifetimes with relative amplitudes in parentheses: 100 ps (23%) and ≫1 ns (77%) at 2040 cm^{-1} and ∼2 ns (100%) at 2070 cm^{-1}.

4. Discussion

ReCO in DMF Solution. The primary features in the transient absorption spectra of the ReCO complex in DMF after 12 ps, shown in Figure 1a, are the three ground-state bleach peaks at 1899, 1914, and 2019 cm^{-1} and the corresponding three

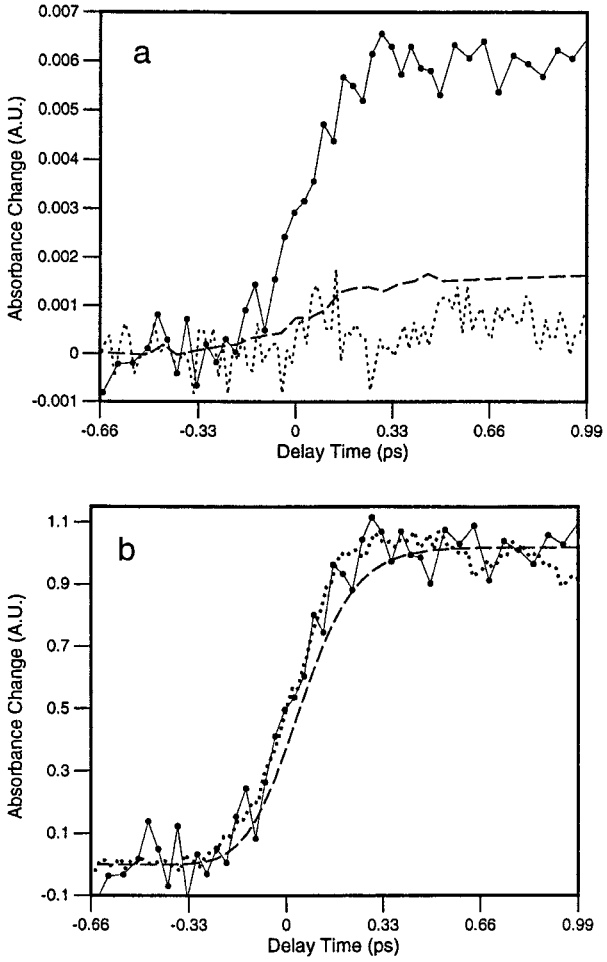

Figure 7. (a) Comparison of signals in nanocrystalline thin films of ReCO on TiO_2 (solid line), ReCO on ZrO_2 (dotted line), and naked TiO_2 (dashed line) probed at 2115 cm^{-1} after 400-nm excitation. (b) Comparison of the normalized signal rise time in ReCO on a TiO_2 film probed at 2115 cm^{-1} (solid circles) with the instrument response function measured in a thin silicon wafer (dotted line) and a 100-fs exponential rise convolved with the instrument response function (dashed line).

excited-state absorption peaks at 1959, 1998, and 2073 cm^{-1}. The excited-state absorption bands are blue-shifted by 50−80 cm^{-1} relative to the ground-state absorption. The primary optical transition excited at 400 nm is a d-to-π^* MLCT transition from the Re(I) metal center to the π^* orbital of the dcbpy ligand.[39,40] This transition effectively oxidizes the Re(I) metal center to Re(II), which reduces the electron density on the metal center. This reduction in the electron density diminishes the metal center's ability to undergo π back-bonding to the CO π^* orbital, which reduces the electron density of this orbital and increases the vibrational frequency.[41−43] A blue shift of the CO stretching frequencies in a similar complex, $Re(CO)_3Cl(bpy)$ (bpy = 2,2′-bipyridine) in acetonitrile, has been observed by Clark and co-workers.[41,44] They observed 50−80 cm^{-1} blue shifts in the CO stretching peaks in the lowest ^{3}MLCT excited state compared to those in the ground state. Similar blue shifts were also observed in the complex $Re(CO)_3Cl(4,4'\text{-bipyridine})_2$.[42,43]

These excited-state peaks appear to blue shift to their final positions in <12 ps, as illustrated in Figure 1b. The rise time of the peak at 2073 cm^{-1} can be described by a single-exponential rise time of about 4 ps, shown in Figure 4. There are at least two possible reasons for the early-time spectral evolution of ReCO in DMF. Both vibrational relaxation in and solvation of the MLCT state can lead to this spectral evolution.

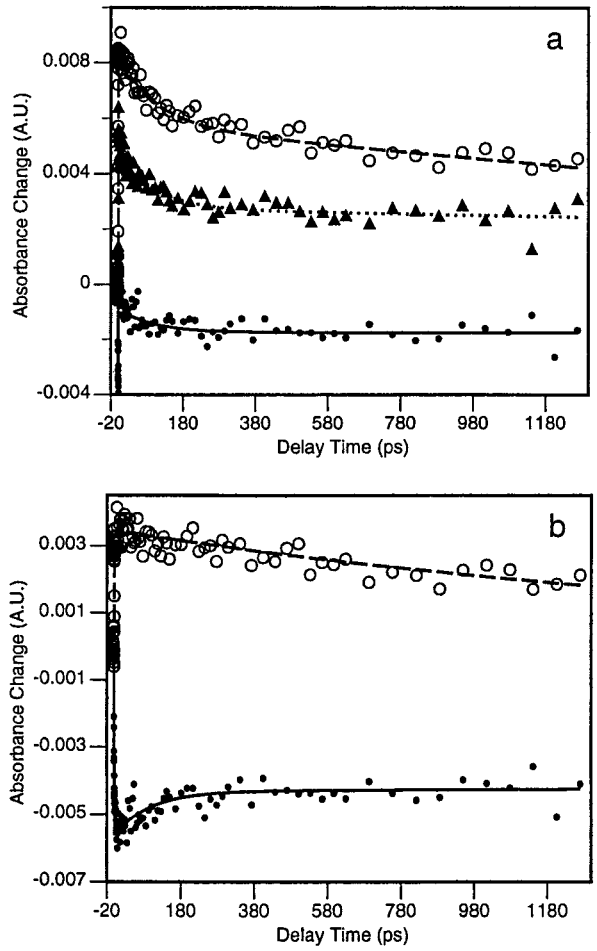

Figure 8. (a) Decay kinetics of transient IR signals measured in ReCO on a TiO_2 nanocrystalline thin film at 2040 (solid circles), 2070 (open circles), and 2115 cm^{-1} (solid triangle). (b) Bleach-recovery kinetics at 2040 cm^{-1} (solid circles) and excited-state decay at 2070 cm^{-1} (open circles) are obtained by subtracting the kinetics at 2115 cm^{-1} from the kinetics at these frequencies.

Optical excitation at 400 nm excites the molecule to a level that is about 10 000 cm^{-1} higher in energy than the lowest vibrational level of the relaxed long-lived ^{3}MLCT state. Highly vibrationally excited molecules often show broadened CO stretching bands because of anharmonic coupling with highly excited low-frequency modes. Cooling of the excess vibrational energy often leads to the narrowing and blue shifting of the CO stretching bands.[45−49] The possible contribution of solvation dynamics to the spectral evolution will be discussed in the following section, where it is compared to the spectral evolution of ReCO on the ZrO_2 film.

The bleach-recovery and absorption-decay dynamics at different peaks are frequency-dependent at early times because of the evolution of the excited-state absorption bands and their overlap with the ground-state bleach.[46] We selected the bleach at 1899 cm^{-1}, the peak of the lowest-frequency band shown in Figure 2a, to monitor the ground-state bleach recovery because, at this frequency, the bleach appears to have negligible overlap with the excited-state absorption bands. We chose the excited-state absorption at 2073 cm^{-1}, the peak of the highest-frequency band shown in Figure 2b, to describe the excited-state dynamics. The excited-state decay was fit to a single-exponential function having a lifetime of 10 ns. This lifetime is consistent with a 15-ns fluorescence lifetime observed in a similar complex in 2-methyltetrahydrofuran.[39] There appears to be a larger magnitude of the ground-state bleach recovery than of the excited-state absorption decay of the traces shown in panels a and b of Figure 2. However, the trend is not the same for different bands. We attribute the different kinetics to the different amount of spectral overlap with excited-state absorptions at early times and to the noise and limited time delay of the data.

ReCO on a ZrO_2 Film. The transient absorption spectra of the ReCO complex adsorbed to the surface of a ZrO_2 nanocrystalline thin film, shown in panels a and b of Figure 3, share many similar features with the transient absorption spectra of ReCO in DMF. There are three prominent ground-state bleach peaks at 1917, 1944, and 2044 cm^{-1}. Just as for ReCO in DMF, the excited-state absorptions of the complex on the ZrO_2 film around 1990 cm^{-1} and at 2069 cm^{-1} are also blue-shifted relative to their corresponding ground-state absorptions. However, there are a few major differences to point out between these two sets of transient spectra of ReCO in different environments. For ReCO on the ZrO_2 film, (1) the magnitudes of the spectral blue shifts in the excited state are smaller, (2) the rate of excited-state spectral evolution appears to be faster, and (3) the lifetime of the excited state is shorter.

Magnitudes of the CO Stretching Frequency Shifts. The ground-state CO stretching frequencies for ReCO on ZrO_2 are higher than those for ReCO in DMF because of the different solvent environments. This red shift of the CO stretching frequency in solvent relative to that in gas phase has been observed for most metal carbonyls. More interestingly, the magnitudes of the blue shifts of the CO stretching frequency in the excited state relative to that in the ground state are much smaller for ReCO on the ZrO_2 film than those for ReCO in DMF solution. For example, the well-separated high-frequency mode of ReCO on ZrO_2 is shifted by about 25 cm^{-1} to the final position of 2069 cm^{-1} in the excited state, which is much smaller than the corresponding shift of about 54 cm^{-1} for ReCO in DMF. The difference between the blue shifts of the CO stretching frequencies on the ZrO_2 film and in DMF solution might result from the different solvent environments because the ZrO_2 film essentially has no solvent. A similar phenomenon was observed when $Re(CO)_3Cl(bpy)$ (bpy = 2,2′-bipyridine) was studied in fluid solution and in a glass matrix by Clark et al.[44] They observed a smaller blue shift of the excited-state peaks in the matrix and attributed it to the lack of solvation of the MLCT state in the matrix environment. Our results are consistent with their observation. DMF has a strong dipole for stabilizing the charge-transfer excited state, whereas the ZrO_2 film has no solvent. Thus, the excited state of ReCO in ZrO_2 is not fully solvated and has less of a blue shift in the CO stretching frequency.

Dynamics of the Spectral Shift. Another difference between the transient spectra of ReCO on the ZrO_2 film compared to those of ReCO in the DMF solution is the rate of spectral evolution observed at the early times. As shown in Figures 1b, 3b, and 4, the high-frequency peak appears to reach its final position much faster on the ZrO_2 thin film than in DMF solution. The source of the difference in the spectral evolution of the transient absorption spectra of ReCO can come from two effects: (1) The bands of ReCO on the ZrO_2 film are much broader than those of ReCO in DMF, which will tend to obscure any spectral changes. (2) There is no solvent in the ZrO_2 film, so that solvation dynamics cannot affect the excited-state absorption spectrum. A Gaussian fit of the high-frequency ground-state bleaches of ReCO on the ZrO_2 film and in DMF shows that the bleach peak is about 4 times broader on ZrO_2. The broadened line shapes observed on the ZrO_2 film are

attributed to an inhomogeneous distribution of binding sites on the film. It is reasonable to assume that ReCO on ZrO_2 films would have excess vibrational energy and a redistribution rate similar to those of ReCO in DMF as a result of 400-nm excitation. Therefore, any differences in the spectral evolution that do not result from the broader line shapes of the peaks for ReCO on the ZrO_2 film probably result from solvation dynamics that occur only in the DMF solution. The components of the solvation time in DMF have been measured to be about 0.82 and 4.72 ps by Chang et al.[50] and 0.40 (55%) and 2.5 ps (45%) by Barbara et al.[51] The slow component of this solvation time is similar to the 4-ps formation time of the absorption at 2073 cm^{-1}, shown as in Figure 4. An ongoing solvent-dependence study should help to test the validity of this assignment and to quantify the extent of the spectral shift caused by solvation.

Excited-State Quenching Dynamics. Two additional differences between the ReCO complex adsorbed on the surface of a ZrO_2 nanocrystalline thin film and ReCO in DMF are the bleach-recovery and absorption decay rates. The difference between the excited-state decay rates of ReCO in the two environments can clearly be seen in the decay of the high-frequency absorption peaks in Figures 1a and 3a. The shorter excited-state lifetime of ReCO on the ZrO_2 film may result from the quenching of excited molecules by each other because of the proximity of the molecules on the ZrO_2 film surface.[52] This proximity allows energy transfer to occur between neighboring molecules. If energy transfer occurred between a molecule in its excited state and a molecule in its ground state, thereby exciting the second molecule and relaxing the first, then the energy would have effectively moved to a new position but no excited-state population would have been lost. We cannot observe this type of energy transfer as our absorbance measurements are sensitive to only the concentrations of the ground and excited states, which would remain unchanged in the above energy-transfer process. However, if quenching between excited molecules occurred, then the excited-state decay rate would change as a function of the concentration of the excited state. Therefore, a pump-power dependence would be observed. Two commonly considered bimolecular excited-state quenching processes are given by eqs 1 and 2.[53]

$$^3M^* + {}^3M^* \rightarrow {}^1M^* + {}^1M \quad (1)$$

$$^3M^* + {}^3M^* \rightarrow {}^3M^{**} + {}^1M \quad (2)$$

Only the $^3M^*$ excited states are considered to be reactants in the bimolecular quenching reaction because the intersystem crossing rate is thought to be very fast in similar transition-metal complexes.[54−56] In eq 1, a singlet excited state of the molecule is re-formed from two triplet excited states. The newly formed singlet excited state quickly relaxes to the triplet state, resulting in the quenching of one of the triplet excited states. In eq 2, a higher-lying triplet excited state is formed. This state quickly relaxes to the lowest-lying triplet state and, again, results in the quenching of one of the triplet excited states.

To investigate whether this type of bimolecular excited-state quenching occurred among ReCO molecules on the ZrO_2 film surface, we measured the excited-state decay and bleach-recovery kinetics at three different pump energies. As shown in panels a and b of Figure 5, the lifetimes of the single-exponential fits to the bleach-recovery traces at 2044 cm^{-1} and the absorption-decay traces at 2069 cm^{-1} are 1.5, 4, and 7 ns for excitation energies of 10, 5, and 2 μJ, respectively. The general trend is that the 2- and 5-μJ traces show similar dynamics within the limit of the noise, whereas the 10-μJ traces at both frequencies show significantly faster excited-state decay and bleach recovery. Although the data are too noisy to extract any quantitative information about the decay rates, it is clear that the excited state was quenched faster at the 10-μJ pump energy than at the lower pump energies. We therefore conclude that the observed pump-energy-dependent decay is consistent with a bimolecular excited-state quenching process between ReCO molecules adsorbed to the surface of the ZrO_2 film.

In a recent study of RuN3-sensitized ZnO nanocrystalline thin films,[33] we suggested that excited-state quenching competed with electron injection from the ^{3}MLCT state of RuN3 to ZnO. We observed a decrease in the magnitude of the injected-electron absorption signal in films with higher surface concentrations of RuN3 under the same excitation energy. Because the electron injection occurred on the 100-ps time scale in this system, we reasoned that the decrease in the magnitude of the electron absorption signal at higher surface concentrations resulted from quenching of excited states that were close together, presumably in the same aggregate. The results of the ReCO on ZrO_2 study provide direct evidence for this type of quenching of photoexcited sensitizer molecules on the surface of nanocrystalline thin films on the <1-ns time scale. Excited-state quenching on longer time scales has been observed by several groups in many systems over the years.[52,57,58] Excited-state quenching was observed by Ghosh and Bard[57] in a study of $Ru(bpy)_3^{2+}$ in colloidal clay suspensions. They found that the emission lifetime of the complex varied with the excitation intensity, and they attributed this dependence to bimolecular excited-state quenching. Also, Kamat and co-workers have found surface-coverage and excitation-intensity dependencies in energy transfer between molecules on surfaces.[52,58]

ReCO on a TiO_2 Film. *Electron Injection.* The transient absorption spectra of the ReCO complex on a TiO_2 nanocrystalline thin film, shown in Figure 6, consist of the vibrational features of the complex superimposed onto a broad absorption, indicated by the thin dotted lines. The rise time and signal magnitude of the broad absorption are the same within the limit of the noise from 2100 to 2200 cm^{-1} (result not shown), a frequency region devoid of the complex's vibrational features. We have observed this type of broad transient absorption signal of injected electrons in several systems in which electron transfer occurs from the adsorbate to TiO_2.[10−12,31,32] Therefore, the broad absorption in Figure 6 is evidence that electrons were injected into the TiO_2 film from the complex. The excited-state energy of a similar ReCO complex, $Re(CO)_3Cl(bpy\text{-}COOEt)$ (bpy-COOEt = 2,2′-bipyridine-4,4′-diethylester), is estimated to be about −0.35 eV (vs SSCE) from the band origin of 14 300 cm^{-1},[39] which was estimated from the overlap of the absorption and emission spectra and the ground-state reduction potential of 1.42 V.[39] We have assumed the same energetics for our ReCO complex. The relaxed excited state may not be able to inject electrons into TiO_2. However, upon absorption of a 400-nm photon, the Franck−Condon state that is populated has an energy that is 3.1 eV higher than that of the ground state or a redox potential of −1.68 V (vs SSCE). At this energy, which is above the conduction band edge of TiO_2 [at about −0.5 V (vs SSCE)],[4] the Franck−Condon state can inject an electron into TiO_2 if the electron injection can compete with the excited-state relaxation process. Electron injection from a vibrationally hot state to TiO_2 was suggested in previous studies of RuN3-sensitized TiO_2.[12,15]

To further confirm the source of the broad absorption, we compared the transient absorption signal in ReCO-sensitized

TiO_2 with those from two blank samples, from ReCO on a ZrO_2 film, and from the naked TiO_2 film, at several frequencies removed from the ground- and excited-state vibrational features of ReCO. Figure 7a shows a comparison of ReCO on the TiO_2 film with the two blank samples at 2115 cm^{-1}. There appears to be negligible transient absorption resulting from ReCO on the ZrO_2 film. In addition, the naked TiO_2 film only contributes a small signal. The signal from direct excitation of the TiO_2 film should be even smaller in the sensitized films because the absorption of ReCO onto the film reduces the number of pump photons that can be absorbed directly by TiO_2.

Figure 7b shows the normalized kinetics at 2115 cm^{-1} compared to the instrument response function measured in a thin silicon wafer, which represents an instantaneous rise. For comparison, a function representing a convolution of the instrument response function with a 100-fs exponential rise is also shown in Figure 7b. From this comparison, the rise time appears to be less than 100 fs. Because the relaxed excited state lies below the conduction band edge, electron injection must occur prior to or in competition with the excited-state relaxation. Therefore, the rise time of the electron signal depends on both the electron-transfer rate and the excited-state relaxation rate. Although we cannot obtain the electron-injection time directly, the fact that electron injection occurs suggests that the injection rate is comparable to the vibrational relaxation time in the excited state. A detailed analysis of the competition of electron injection and relaxation and the effect on electron-absorption rise kinetics and quantum yield will be presented in future publications. The electron-injection time of a similar complex, RuN3, has been observed to occur on a similar ultrafast time scale by many groups.[10−13,15,17] Although the reason for the ultrafast electron injection is unclear in RuN3 and in ReCO, both complexes share a MLCT transition[8,39,40] to the dcbpy ligand, which is bound strongly to the TiO_2 surface through the anchoring carboxylic acid groups.[59] It has been reasoned that the MLCT transition promotes an electron to the π^* orbital of the dcbpy ligand, which is in intimate contact with the TiO_2 surface. The favorable mixing of the accepting states of the TiO_2 surface and the donating state of the dcbpy ligand results in ultrafast electron injection.

Adsorbate Vibrational Spectra. In addition to the dominating broad absorption signal from the injected electrons, vibrational features of the adsorbate molecules can also be observed in the transient spectra. The ground-state bleach peak at 2040 cm^{-1} corresponds well with the ground-state peaks shown in the static FTIR spectrum. The transient absorption spectrum of ReCO on the ZrO_2 film at 831 ps was also included in Figure 6 to facilitate assignment of the excited-state absorption peaks. This spectrum has been red shifted to match the ground-state absorption bands of the complex on TiO_2. From the comparison, the band at around 2070 cm^{-1} can be assigned to the excited-state absorption. In addition, the new peak at about 2095 cm^{-1} can be assigned to the high-frequency CO stretching band of the oxidized form of the ReCO complex, as this peak is not present in the spectra of the complex on the ZrO_2 film, a noninjecting substrate. When an electron is injected from the π^* orbital of the dcbpy ligand into the TiO_2 film, a small decrease in the electron density around the metal center is expected because of the mixing of the π^* orbital of dcbpy and the metal d orbitals. As a result, the oxidized ReCO should have a CO stretching frequency further blue-shifted relative to that in the MLCT excited state.

As shown in Figure 6, a large percentage of the molecules are still in the excited state in the time range of 500−1000 ps, as indicated by the absorption peak at 2070 cm^{-1}, a time scale that is much longer than the <100-fs electron-injection time. This fact indicates that the quantum yield for electron injection from the complex into the TiO_2 film is not unity and that electron injection does not occur from the relaxed excited state. This result again suggests that electron injection may have occurred from a vibrationally hot state. Future measurements with much improved signal-to-noise levels may lead to an accurate determination of the dynamics of the excited state and of oxidized ReCO. By comparing these dynamics with those of electron absorption inside the nanoparticle, we hope to gain a detailed understanding of the injection process.

The ground-state bleach recovery of ReCO on TiO_2 was obtained by subtracting the dynamics observed at the bleach-peak frequency, 2040 cm^{-1}, from the dynamics observed far from the bleach peak, at 2115 cm^{-1}, as shown in Figure 8a. We assume that the dynamics at 2115 cm^{-1} are free of interference from any vibrational features of ReCO in its ground-state, excited-state, or oxidized forms. As shown in Figure 8b, the subtracted kinetics at 2040 cm^{-1}, representing the bleach recovery, show a small (23%) fast-recovery component with a time constant of 100 ps. There are several possible explanations for the fast bleach recovery. Given the fact that we have observed excited-state quenching of the ReCO complex on a ZrO_2 film, the quenching mechanism may be the most plausible explanation. One would expect a corresponding fast component in the excited-state decay kinetics. Unfortunately, the signal-to-noise level of the excited-state decay kinetics at 2070 cm^{-1} is not sufficient to clearly prove or disprove this notion. Another possibility is that we are observing back electron transfer from the TiO_2 film to the Re center of the oxidized ReCO, which would re-form the ground state. However, this explanation is less plausible because of the extremely slow back electron transfer measured in RuN3-sensitized TiO_2.[17,29] In RuN3, the bipyridine ligand may serve both as a bridge to facilitate electron transfer in the excited state and as a barrier to inhibit back electron transfer to the oxidized metal center. Because of the similarities in the structure and probable binding geometry of these two complexes, we expect that ReCO will exhibit similarly slow back electron transfer from the TiO_2 film to the oxidized Re center.

5. Summary

We have directly observed the excited-state dynamics of $Re(CO)_3Cl(dcbpy)$ in DMF solution and on the surface of nanocrystalline ZrO_2 and TiO_2 thin films. For $Re(CO)_3Cl(dcbpy)$ in DMF solution, a long-lived excited state with a lifetime of >1 ns was observed after 400-nm excitation of the ^{1}MLCT band. In this excited state, which is assigned to the ^{3}MLCT state, the CO stretching bands are blue-shifted compared to their corresponding ground-state absorption peaks. These excited-state bands fully developed after 12 ps as a result of vibrational relaxation and/or solvation. On the surface of the ZrO_2 thin film, a similar ^{3}MLCT excited state was observed, although the magnitudes of the blue shifts in CO stretching frequencies were much smaller. The large difference in the frequency shifts is attributed to the lack of solvation of the MLCT state for $Re(CO)_3Cl(dcbpy)$ on the ZrO_2 film. This notion appears to be supported by the slower rate for the excited-state spectral shift for $Re(CO)_3Cl(dcbpy)$ in solution. The lifetime of the ^{3}MLCT for ReCO on ZrO_2 was found to be much shorter than that for the molecule in solution. The excited-state lifetime decreased with increasing excitation power, suggesting that there is significant quenching between excited-state molecules that are

in proximity in the film. For $Re(CO)_3Cl(dcbpy)$-sensitized TiO_2 nanocrystalline thin films, a broad IR absorption of injected electrons was observed after 400-nm excitation. The rise time of the electron absorption signal was estimated to be in the <100-fs time range. In addition, the CO stretching modes of the adsorbate in the ground state, the excited state, and the oxidized form were observed. The $Re(CO)_3Cl(dcbpy)$ complex may serve as a model complex for the Ru polypyridyl complexes that have shown great potential as efficient sensitizers for solar cells based on TiO_2 nanocrystalline thin film electrodes. The strong CO stretching bands will allow us to monitor the dynamics of the adsorbate, in addition to monitoring the injected electrons, to learn more about the detailed mechanism of electron injection. Experiments toward this goal are ongoing.

Acknowledgment. We are grateful for financial support from the Chemical Science Division, U.S. Department of Energy (Grant DE-FG02-98ER14918). This work is also supported in part by the Petroleum Research Fund, administered by the American Chemical Society, and the Emory University Research Committee.

References and Notes

(1) Miller, R. J. D.; McLendon, G. L.; Nozik, A. J.; Schmickler, W.; Willig, F. *Surface Electron-Transfer Processes*; VCH Publishers: New York, 1995.
(2) Nozik, A. J.; Memming, R. *J. Phys. Chem.* **1996**, *100*, 13061.
(3) Kamat, P. V. *Prog. React. Kinet.* **1994**, *19*, 277−316.
(4) Hagfeldt, A.; Gratzel, M. *Chem. Rev.* **1995**, *95*, 49−68.
(5) Jacobson, K. I.; Jacobson, R. E. *Imaging Systems*; John Wiley & Sons: New York, 1976.
(6) Kay, A.; Gratzel, M. *Sol. Energy Mater. Sol. Cells* **1996**, *44*, 99−117.
(7) Serpone, N. *Res. Chem. Intermed.* **1994**, *20*, 953−992.
(8) Nazeeruddin, M. K.; Kay, A.; Rodicio, I.; Humphrybaker, R.; Muller, E.; Liska, P.; Vlachopoulos, N.; Gratzel, M. *J. Am. Chem. Soc.* **1993**, *115*, 6382−6390.
(9) Oregan, B.; Gratzel, M. *Nature* **1991**, *353*, 737−740.
(10) Asbury, J. B.; Ghosh, H. N.; Ellingson, R. J.; Ferrere, S.; Nozik, A. J.; Lian, T. Femtosecond IR Study of Ru Dye Sensitized Nanocrystalline TiO_2 Thin Films: Ultrafast Electron Injection and Relaxation Dynamics. In *Ultrafast Phenomena XI*; Elasser, T., Fujimoto, J. G., Wiersma, D., Zinth, W., Eds.; Springer-Verlag: Berlin, 1998; p 639.
(11) Ellingson, R. J.; Asbury, J. B.; Ferrere, S.; Ghosh, H. N.; Lian, T.; Nozik, A. J. *J. Phys. Chem. B* **1998**, *102*, 6455.
(12) Asbury, J. B.; Ellingson, R. J.; Ghosh, H. N.; Ferrere, S.; Nozik, A. J.; Lian, T. *J. Phys. Chem. B* **1999**, *103*, 3110−3119.
(13) Heimer, T.; Heilweil, E. J. *J. Phys. Chem. B* **1997**, *101*, 10990−10993.
(14) Heimer, T.; Heilweil, E. J. Measuring Ultrafast Sensitizer−TiO_2 Electron Dynamics with Mid-Infrared Spectroscopy. In *Ultrafast Phenomena XI*; Elsasser, T., Fujimoto, J. G., Wiersma, D., Zinth, W., Eds.; Springer-Verlag: Berlin, 1998; p 505.
(15) Hannappel, T.; Burfeindt, B.; Storck, W.; Willig, F. *J. Phys. Chem. B* **1997**, *101*, 6799−6802.
(16) Eichberger, R.; Willig, F. *Chem. Phys.* **1990**, *141*, 159−173.
(17) Tachibana, Y.; Moser, J. E.; Gratzel, M.; Klug, D. R.; Durrant, J. R. *J. Phys. Chem.* **1996**, *100*, 20056−20062.
(18) Yan, S. G.; Hupp, J. T. *J. Phys. Chem. B* **1997**, *101*, 1493−1495.
(19) Yan, S. G.; Hupp, J. T. *J. Phys. Chem.* **1996**, *100*, 17.
(20) Zaban, A.; Ferrere, S.; Gregg, B. A. *J. Phys. Chem. B* **1998**, *102*, 452.
(21) Zaban, A.; Ferrere, S.; Sprague, J.; Gregg, B. A. *J. Phys. Chem. B* **1997**, *101*, 55.
(22) Vinodgopal, K.; Hua, X.; Dahlgren, R. L.; Lappin, A. G.; Patterson, L. K.; Kamat, P. V. *J. Phys. Chem.* **1995**, *99*, 10883−10889.
(23) Fessenden, R. W.; Kamat, P. V. *J. Phys. Chem.* **1995**, *99*, 12902−12906.
(24) Argazzi, R.; Bignozzi, C. A.; Heimer, T. A.; Castellano, F. N.; Meyer, G. J. *J. Phys. Chem. B* **1997**, *101*, 2591−2597.
(25) Heimer, T. A.; Darcangelis, S. T.; Farzad, F.; Stipkala, J. M.; Meyer, G. J. *Inorg. Chem.* **1996**, *35*, 5319−5324.
(26) Ford, W. E.; Rodgers, M. A. J. *J. Phys. Chem.* **1994**, *98*, 3822.
(27) Hannappel, T.; Zimmermann, C.; Meissner, B.; Burfeindt, B.; Storck, W.; Willig, F. *J. Phys. Chem. B* **1998**, *102*, 3651.
(28) Moser, J. E.; Noukakis, D.; Bach, U.; Tachibana, Y.; Klug, D.; Durrant, J. R.; Humphry-Baker, R.; Gratzel, M. *J. Phys. Chem. B* **1998**, *102*, 3649.
(29) Haque, S. A.; Tachibana, Y.; Klug, D. R.; Durrant, J. R. *J. Phys. Chem. B* **1998**, *102*, 1745−1749.
(30) Asbury, J. B.; Wang, Y. Q.; Ghosh, H. N.; Lian, T. Manuscript in preparation.
(31) Ghosh, H. N.; Asbury, J. B.; Lian, T. *J. Phys. Chem. B* **1998**, *102*, 6482−6486.
(32) Ghosh, H. N.; Asbury, J. B.; Weng, Y.; Lian, T. *J. Phys. Chem. B* **1998**, *102*, 10208.
(33) Asbury, J. B.; Wang, Y. Q.; Lian, T. *J. Phys. Chem. B* **1999**, *103*, 6643.
(34) Cavicchia, M. A.; Alfano, R. R. Ultrafast Upper Sattelite Valley Spectroscopic Dynamics Using UV Pump−IR Probe Absorption Spectroscopy in GaAs and GaP. In *Ultrafast Phenomena in Semiconductors*; Ferry, D. K., van Driel, H. M., Eds.; Society of Photo-Optical Instrumentation Engineers: Bellingham, WA, 1994; Vol. 2142, p 128.
(35) Woerner, M.; Elsaesser, T.; Kaiser, W. *Phys. Rev. B* **1992**, *45*, 8378.
(36) Faist, J.; Capasso, F.; Sivco, D. L.; Sirtori, C.; Hutchinson, A. L.; Cho, A. Y. *Science* **1994**, *264*, 553.
(37) Pankove, J. I. *Optical Processes in Semiconductors*; Dover Publications: Mineola, NY, 1975.
(38) Wang, Y.; Lian, T. Manuscript in preparation.
(39) Worl, L. A.; Duesing, R.; Chen, P.; Ciana, L. D.; Meyer, T. J. *J. Chem. Soc., Dalton Trans.* **1991**, 849−858.
(40) Wrighton, M.; Morse, D. L. *J. Am. Chem. Soc.* **1974**, *96*, 998−1003.
(41) George, M. W.; Turner, J. J. *Coord. Chem. Rev.* **1998**, *177*, 201−217.
(42) Turner, J. J.; George, M. W.; Johnson, F. P. A.; Westwell, J. R. *Coord. Chem. Rev.* **1993**, *125*, 101−114.
(43) Gamelin, D. R.; George, M. W.; Glyn, P.; Grevels, F. W.; Johnson, F. P. A.; Klotzbucher, W.; Morrison, S. L.; Russell, G.; Schaffner, K.; Turner, J. J. *Inorg. Chem.* **1994**, *33*, 3246−3250.
(44) Clark, I. P.; George, M. W.; Johnson, F. P. A.; Turner, J. J. *J. Chem. Soc., Chem. Commun.* **1996**, 1587.
(45) Arrivo, S. M.; Dougherty, T. P.; Grubbs, W. T.; Heilweil, E. J. *Chem. Phys. Lett.* **1995**, *235*, 247−254.
(46) Dougherty, T. P.; Heilweil, E. J. *Chem. Phys. Lett.* **1994**, *227*, 19−25.
(47) Grubbs, W. T.; Dougherty, T. P.; Heilweil, E. J. *Chem. Phys. Lett.* **1994**, *227*, 480−484.
(48) Lian, T. Q.; Bromberg, S. E.; Asplund, M. C.; Yang, H.; Harris, C. B. *J. Phys. Chem.* **1996**, *100*, 11994−12001.
(49) Asbury, J. B.; Ghosh, H. N.; Yeston, J. S.; Bergman, R. G.; Lian, T. Q. *Organometallics* **1998**, *17*, 3417−3419.
(50) Chang, Y. J.; Castner, E. W. *J. Phys. Chem.* **1994**, *98*, 9712−9722.
(51) Barbara, P. F.; Jarzeba, W. *Adv. Photochem.* **1990**, *15*, 1.
(52) Kamat, P. V. *Chem. Rev.* **1993**, *93*, 267−300.
(53) Birks, J. B. *Photophysics of Aromatic Molecules*; John Wiley & Sons: London, 1970.
(54) Damrauer, N. H.; Cerullo, G.; Yeh, A.; Boussie, T. R.; Shank, C. V.; McCusker, J. K. *Science* **1997**, *275*, 54.
(55) McCusker, J. K.; Walda, K. N.; Dunn, R. C.; Simon, J. D.; Magde, D.; Hendrickson, D. N. *J. Am. Chem. Soc.* **1992**, *114*, 6919−6920.
(56) McCusker, J. K.; Walda, K. N.; Dunn, R. C.; Simon, J. D.; Magde, D.; Hendrickson, D. N. *J. Am. Chem. Soc.* **1993**, *115*, 298−307.
(57) Ghosh, P. K.; Bard, A. J. *J. Phys. Chem.* **1984**, *88*, 5519−5526.
(58) Liu, D.; Hug, G. L.; Kamat, P. V. *J. Phys. Chem.* **1995**, *99*, 16768−16775.
(59) Duffy, N.; Dobson, K. D.; Gordon, K. C.; Robinson, B. H.; McQuillan, A. J. *Chem. Phys. Lett.* **1997**, *266*, 451−455.